

Dehydroxylation of Kaolinite to Metakaolin – A Molecular Dynamics Study

Shani Sperinck,^{*a} Paolo Raiteri,^a Nigel Marks^a and Kate Wright^a

^a Nanochemistry Research Institute, Department of Chemistry, Curtin University, GPO Box U1987, Perth, WA, 6845, Australia. Fax: +61 8 9266 3780; Tel: +61 8 9266 3780; E-mail: s.sperinck@curtin.edu.au

The thermally induced transformation of kaolinite to metakaolin is simulated using molecular dynamics through a step-wise dehydroxylation approach. The simulation shows that the removal of structural water through dehydroxylation produces a distortion or buckling effect in the 1:1 Al-Si layers, which is due to the migration of the aluminium into vacant sites provided by the inter-layer spacing. The structural change is characterized by a loss of crystallinity and a concomitant change in aluminium coordination from octahedral to tetrahedral, with this study confirming the presence of 5-fold aluminium within the metakaolin structure. The degree and probability of Al migration is proportional to the amount of local disorder within the structure, which is governed by the degree of local hydroxyl group loss. This results in the formation of aluminium clusters within the layers. This study proposes that instead of a uniform structure, metakaolin exhibits regions of differing aluminium concentrations, which can have major effects in the reaction chemistry at those sites.

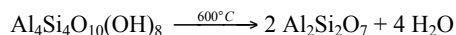
Introduction

The calcination of clay minerals has attracted much interest due to the widespread use of these materials in a diverse range of applications. Of particular interest is the ‘drying’ of clay, which is often the slowest stage in the production of ceramics. To accelerate the process it is necessary to fully understand the mechanisms that govern dehydration. Research has generally focused on the dehydration behaviour of the group of clay minerals classified as 2:1 dioctahedral aluminous phyllosilicates, such as the smectites, montmorillonites, illites and vermiculites¹⁻⁹. Typically the dehydroxylation of these materials is produced by a combination of two independent processes that occur in the calcination process^{1,10-15}: (1) the continuous loss of interlayer water (*dehydration*) and (2) the discontinuous loss of structural water (*dehydroxylation*). This second process results in a strong decrease in the basal distance and is associated with the collapse of the interlayer space and the majority of the structural changes which consequently occur. However, efforts to fully understand the dehydroxylation process have been problematic, as differentiating between the water driven out by each process is difficult¹².

Kaolinite, $\text{Al}_4[\text{Si}_4\text{O}_{10}](\text{OH})_8$, is classified as a 1:1 dioctahedral phyllosilicate and is the main component of the kaolin group of minerals. Kaolins are utilized in a large variety of industrial applications such as ceramics, filling agent in paper, plastics, rubber, cosmetics, etc. The framework structure of kaolinite, shown in Fig. 1, is composed of a sheet of vertex sharing SiO_4 tetrahedra forming six-membered silicate rings that are linked by common oxygen atoms parallel to the *c*-axis to a sheet of edge-sharing AlO_6 octahedra forming four-membered aluminate rings. The silicate and aluminate layers are bound together by strong ionic-covalent bonds via apical oxygen's, and these layers are connected by much weaker hydrogen bonds. This is an idealized structure, as disorder is common in kaolin minerals.

Since a pure kaolinite sample contains no interlayer water, no dehydration step will be present in the calcination process, and the thermally induced structural transformations of kaolinite will be completely governed by the dehydroxylation process.

The calcination of kaolinite has three main thermally induced phases. The first is the process of interest, the endothermic dehydroxylation to the metastable metakaolin phase that occurs in the temperature range of 450 °C to 700 °C according to the following reaction:



Cubic spinel and amorphous silica are produced in the range of 700 °C to 950 °C and the thermodynamically stable mullite phase forms in an exothermic reaction over 1100 °C with crystallization of cristobalite from the amorphous silica phase proceeding beyond that. Whilst the high temperature phases have been the focus of much interest¹⁶⁻²⁰, the metastable is often overlooked due to its non-crystalline nature, and conclusive structural information is limited. Despite this, metakaolin has found widespread use in the food-processing industry, oil shale processing, ceramics, as a pozzolanic material and as a feedstock for geopolymer cement.

Metakaolin is described as x-ray amorphous, but demonstrates two-dimensional regularity in the kaolin layers, which are stacked so that the three-dimensional periodicity is lost. The mechanism of the dehydroxylation process of kaolinite has been the subject of various investigations^{18,20-34} with the general agreement that metakaolin is formed between 300 °C and 700 °C by a gradual loss of structural water through diffusion accompanied by a concomitant change in aluminium coordination from six- to four-fold. In practise, the types and density of the disorder in the starting kaolinite material will result in differences in the final metakaolin structure and residual water content, which can be as much as 12 %wt^{25,31}.

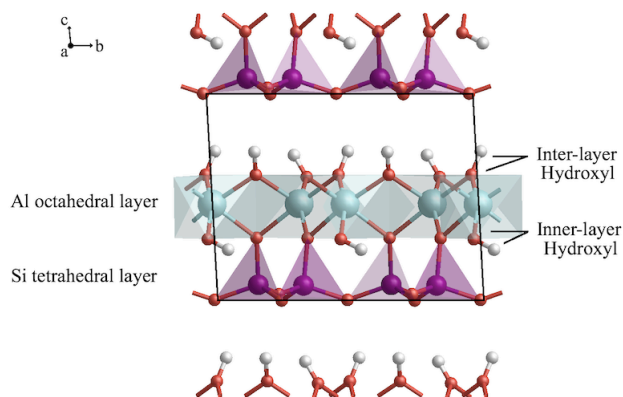


Fig. 1 Ideal layered structure of kaolinite, showing the constructed kaolinite unit cell. The location of the inter- and inner-layer hydroxyls are shown for clarity.

The determination of the structure of metakaolin using computational simulation techniques was recently reported to have made significant progress^{33,34}. The proposed metakaolin structure was obtained by the gradual removal of hydroxyl groups from a kaolinite system, using the first principles approach of density functional theory (DFT). The results showed that through the loss of 87.5% of the water content the octahedral layer demonstrated large structural changes which contributed to a loss in crystalline behaviour. However, there are concerns with the final metakaolin structure produced that must be addressed. The simulation cell used is small (272 atoms) and consequently there is no possibility to simulate long-range disorder. Furthermore, geometry optimization of the system following dehydroxylation restricts the structure to finding the nearest local minimum and the atoms cannot move far from their initial positions. This will not allow the necessary structural reorganisations to occur, and the results reported in this study show that the transformation of kaolinite to metakaolin undergoes significant changes within the layer structure.

This study aims to address these issues by providing complimentary insights into the dehydroxylation of kaolinite to metakaolin on a significantly larger scale. The aim is to determine the atomic mechanisms underpinning the loss of crystallinity and the transformation to metakaolin through the use of a much larger system, higher temperatures and timescales several magnitudes of order greater than the DFT approach could achieve. However, as stated previously, as the size and complexity of the system increases, so does the computational expense. As such, an empirical approach has been implemented to minimise the cost. Although resulting in a loss in the accuracy in the description of the chemical environment, by allowing a much larger system to be studied, the empirical approach imposes less restrictions on the lattice, allowing the collapse of the inter-layer spacing. Thus, by studying the thermal transformation of kaolinite to metakaolin on a larger scale, the mechanisms underpinning the collapse of the interlayer spaces and subsequent structural changes can be further investigated.

Experimental

Model parameters

Computer simulations have become increasingly useful in the study of the atomic structure and behaviour of clays and clay minerals⁷. However, the success of any empirical simulation relies on the accuracy and transferability of the short-range interatomic potentials. The empirical force field potentials for the metal-oxygen interactions used in this work are based on the Teter potential model³⁵, which have been extensively used to model alkali silica glasses³⁶⁻³⁸ and recently crystalline and amorphous zircon³⁹. The interactions of the hydroxyl group are described by an additional Morse potential, which was developed to complete the potential model required for the simulations reported here.

The total potential energy of a system is described by the sum of non-bonded and bonded interactions.

$$E_{\text{Total}} = E_{\text{Bond}} + E_{\text{Nonbond}} \quad (1)$$

For the non-bonded metal-oxygen interactions, the potential energy consists of a simple Buckingham potential coupled with electrostatics.

$$E_{\text{Nonbond}} = A \exp\left(-\frac{r}{\rho}\right) - \frac{C}{r^6} + \frac{q_i q_j}{4\pi\epsilon_0 r} \quad (2)$$

where r is the distance between the atoms i and j , q_i and q_j are the ionic charges, ϵ_0 is the dielectric permittivity of vacuum, and A , ρ and C are constants. Particular care was taken when assigning parameters as the $d_{(001)}$ layer repeat distances of lamellar minerals, which represent the interactions of the octahedral and tetrahedral sheets here, are extremely sensitive to the non-bonded parameters of a force field⁴⁰. For the hydroxyl pairs, a Morse potential function^{41,42} was used

$$E_{\text{Bond}} = D_o \left[\left(1 - e^{-a(r_o - r)} \right)^2 - 1 \right] \quad (3)$$

where r_o is the equilibrium bond distance, D_o is the well depth (defined relative to the dissociated atoms), and a controls the width of the potential well.

The atomic coordinates for the periodic structure of kaolinite were generated on the basis of crystal structure refinement data determined from neutron diffraction studies performed at 1.5 K with well-characterised hydrogen position information⁴³. All atoms were represented as partial charge rigid ions, with 5 kinds of atoms present – Al, Si, O1, O2 and H where the O1 and O2 correspond to structural and hydroxyl oxygen's respectively.

Oxygen and hydroxyl charges generally vary depending on their occurrence in water molecules, OH groups, and bridging and substitution environments. Thus in the potential model used here, the interactions due to the structural oxygen's are described differently to those of the hydroxyl oxygen's.

Table 1 Force field parameters for the simulation

Atomic Charges			
Silicon (Si)	2.400	Hydroxyl Oxygen (O2)	-0.856
Aluminium (Al)	1.800	Hydrogen (H)	0.256
Structural Oxygen (O1)	-1.200		
Non-bonded parameters			
Atomic pair	A (eV)	ρ (Å)	C (eV.Å ⁶)
Al – O1	12201.417	0.195628	31.997
Al – O2	9701.4170		
Si – O1	13702.905	0.193817	54.681
Si – O2	12433.827		
O – O	1844.7548	0.343645	192.58
O – H*	100.00	0.250	0.00
Bonded parameters			
	D _c (eV)	a (Å ⁻¹)	r _o (Å)
O2 – H*	7.0525	1.800	0.94850

* The bonded term dominates for short-range interactions where $r \leq 1.3$ Å; the non-bonded term takes over for interactions beyond this range.

Partial charges were assigned to all atoms, as full formal charge models can generate artificially large Coulombic contributions to the potential and have been shown to strongly influence the interlayer structure and dynamics of clay minerals⁴¹. All potential parameters are given in Table 1.

Since this model has not been previously reported in the modelling of layered aluminosilicate systems, rigorous testing was conducted to ensure its suitability for the purposes of this study. In the transformation of kaolinite to metakaolin, one of the key aspects defining the process is the change of the aluminium from an octahedral to a tetrahedral configuration. This means that the Teter potential model must be able to simulate several coordination environments accurately. This was evaluated by using the potential model to simulate nine different crystal types (see Table 2) in which aluminium is present in 4-fold, 5-fold and 6-fold environments, and silicon is present in 4-fold and 6-fold environments.

The unit cell for each crystal structure was constructed from well-defined experimental parameters, and optimized using the General Utility Lattice Program (GULP)⁴⁴. The calculated structural properties of the resulting systems were then compared with experimentally observed values⁴⁵. All structures tested with the potential model reproduced well the experimental properties with the average difference being typically 1-2% and at most 3.6%. The largest structural discrepancy is that Si-O bonds are too strong, being typically underestimated by up to 3%. This not a major concern as Si-O interactions are not central to the kaolin to metakaolin transformation, as Si remains 4-fold coordinated throughout the process. We can therefore conclude that the Teter potential provides a good description of a variety of aluminosilicate systems, and correspondingly will describe well the structural rearrangement of the Al-Si-O network following dehydroxylation. Combined with the advantage of being able to address timescales many orders of magnitude greater than what is accessible via DFT. As we will show, 100 ps of motion must be followed for the system to equilibrate at each dehydroxylation step; this timescale lies far beyond typical computing resources using DFT. The empirical approach therefore balances the competing demands of chemical accuracy and simulation time.

The final aspect of the potential model that required verification was the maximum cut-off (r_{max}) for all the interactions. A cut-off of 15 Å was chosen after testing showed it as the minimum required to ensure all the structures tested in Table 2, including kaolinite, reproduced the experimental structures. The details of the results can be found in the supplementary information.

Molecular dynamics simulation

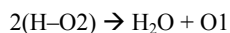
The molecular dynamics (MD) simulations were performed at constant temperature and pressure (NPT) using the DLPOLY code⁴⁶, with the pressure set to 1 atm, temperature to 1000 K and a timestep of 1.0 fs. The temperature and pressure were controlled by the Berendsen method.

Table 2 Structures simulated for potential model verification

Structure simulated	Coordination environment	Average % difference in calculated properties
<i>Al₂SiO₅ Polymorphs</i>		
Andalusite	Al [6] Al [5]	1.29
Kyanite	Al [6] Al [6]	0.43
Sillimanite	Al [6] Al [4]	1.28
<i>SiO₂ Polymorphs</i>		
Quartz	Si [4]	0.75
Stishovite	Si [6]	1.77
Coesite	Si [4]	2.76
Cristobalite	Si [4]	3.59
<i>AlOH</i>		
Gibbsite	Al [6]	1.63
<i>Al₂O₃</i>		
Corundum	Al [4]	2.90

All simulations reported here employed three-dimensional periodic boundary conditions and imposed no space group. The periodic simulation cell constituted a 7x4x5 supercell (4670 atoms) constructed from the optimised kaolinite unit-cell parameters to allow for an approximately cubic structure with dimensions (36.08 x 35.77 x 36.95) Å. The size of the cell was necessary to facilitate the minimum energy convention with a potential model cut-off of 15 Å.

To simulate the dehydroxylation process, the supercell was ‘heated’ to 1000 K. Experimentally the process occurs through a temperature gradient (450 – 700 °C), however, as the exact rates of dehydroxylation through experimental thermal analysis are unknown and would impose too many variables to the simulation, a constant temperature of 1000 K was used in the simulation. Once at temperature, the system was allowed to fully equilibrate and stabilise. At the end of the equilibration period the next H₂O was removed. The liberation of a H₂O molecule was simulated by removing two hydrogen atoms located in neighbouring hydroxyl groups, as well as one of the bonded hydroxyl oxygen atoms. The remaining hydroxyl oxygen is then converted to structural oxygen:



Although an actual H₂O molecule is not simulated, this study will refer to the removed atoms collectively as H₂O.

Since the initial simulation cell contained 1120 hydroxyl groups, or 560 potential H₂O groups, to remove them individually would have required a prohibitively large amount of computational resources. As such, the simulated dehydroxylation was done at a constant rate, with ‘steps’ of 56 potential H₂O groups removed or at a rate of 10% dehydroxylation per step. Typically a period of 100 ps per dehydroxylation step was required for the system to fully equilibrate and stabilise. Thus, each removal step was run for 100 ps at 1000 K, resulting in a total simulation time of just over 1 ns. The dehydroxylation process was continued beyond the experimental threshold of 12% residual water, to a 100% dehydroxylated structure.

The diffusion of the H₂O through the structure was not addressed as the dehydroxylation reaction of kaolinite is not controlled by the physical diffusion of water vapor²⁹.

To minimise thermal noise in the post-simulation analysis, the structure produced at the end of each step was rapidly quenched to 300 K prior to analysis.

The choice of which hydroxyl groups used to make up the H₂O removed was determined randomly, with the only limitation being that the hydroxyls were chosen in a ‘nearest neighbour’ approach i.e. only pairs found within a designated cut-off distance were considered. Several simulations were conducted to determine if the choice of the hydroxyls impacted the final structure obtained. Initially, a comparison was done of the removal of two *inter*-layer hydroxyl groups (Fig. 1) as opposed to two *inner*-layer hydroxyl groups. It was found that it is more energetically favourable to remove H₂O groups from surface hydroxyl pairs than from the inner-layer hydroxyl pairs. This is consistent with observations made in previous studies^{18,47}, although the differences between the changes in energy required are minimal (less than 5%).

To accommodate this, the algorithm used for finding the hydroxyl pairs set an initial cut-off which would preclude the inner-layer hydroxyl groups from participating. Once the dehydroxylation process progressed, this cut-off was increased to allow the inner-layer hydroxyls to be included. The location of the next H₂O group removed was also investigated, with the results showing that regardless of whether two H₂O groups were removed close together or far apart, the energy of the system remains consistent. Finally, the impact of the randomisation of the hydroxyl removal program was tested. The entire dehydroxylation simulation was repeated using the same removals program but starting with a different random number. This results in the locations of the H₂O groups removed differing for the second dehydroxylation simulation than for the first. Although the exact final atomic positions differed in the two structures, the same trends and observations were made in all analysis results as reported here. Further information on these tests can be provided on request.

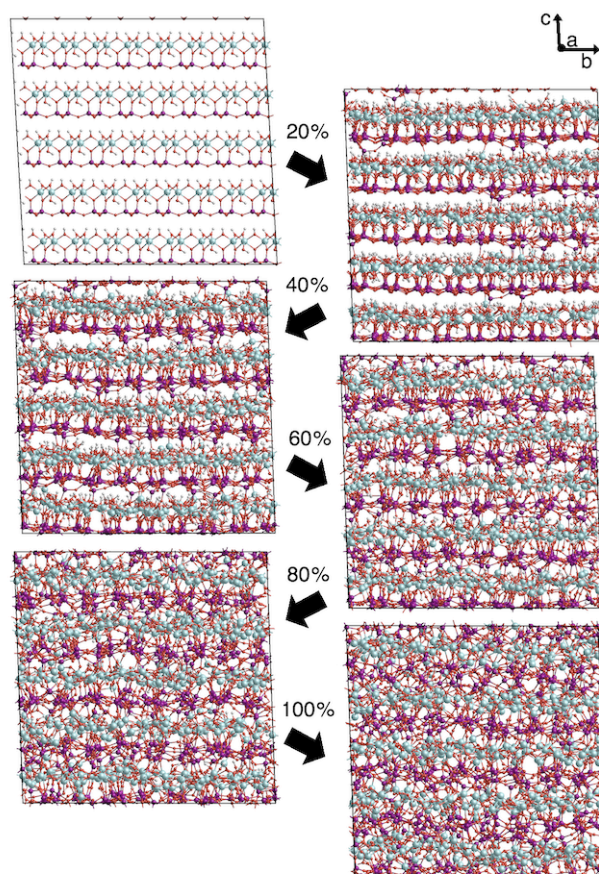


Fig. 2 Snapshots of the dehydroxylation process viewed along the a -axis. Starting from the kaolinite structure (top left), each image shows the quenched structure after 2 removal steps (20% dehydroxylated).

Results and discussion

The chosen kaolinite atomic coordinates were optimised with the tested potential model. This produced the unit cell shown in Fig. 1, which demonstrates the $C1$ symmetry with cell parameters that correspond well with those calculated elsewhere⁴⁸. The calculated bond lengths and angles of the optimized structure corresponded to the experimental ones in all cases except for the Si-O bond lengths, which were shifted towards lower values by up to 2.48%.

A comparison of the calculated structural properties is shown in Table 3, with all results corresponding well with the experimentally determined values.

Table 3 Comparisons of structural properties of kaolinite

Parameter	Experimental ^{40,48}	Calculated	% Difference
a (Å)	5.1535	5.1946	0.80
b (Å)	8.9419	9.0436	1.14
c (Å)	7.3906	7.3788	0.16
α (°)	91.926	92.210	0.31
β (°)	105.056	105.194	0.13
γ (°)	89.797	89.798	0.01
Shear Modulus (GPa)	14.8 – 31.8 ⁴⁹	30.59	-
Bulk Modulus (GPa)	37.5 – 55.5 ⁴⁹	55.24	-

A range of bulk and shear moduli are given for comparison, as despite the many reported measurements of the kaolinite elastic properties found in the literature, there is little agreement between the values reported⁴⁹. Because of the discrepancies it is difficult to compare the calculated properties directly, although the calculated values lie within the upper range of the experimental ones.

The $7 \times 4 \times 5$ supercell was then constructed and the dehydroxylation commenced. The process of structural change through the dehydroxylation process is depicted in Fig. 2. It is evident that as the simulation proceeds the inter-layer space partially collapses, although with the 1:1 layering still present.

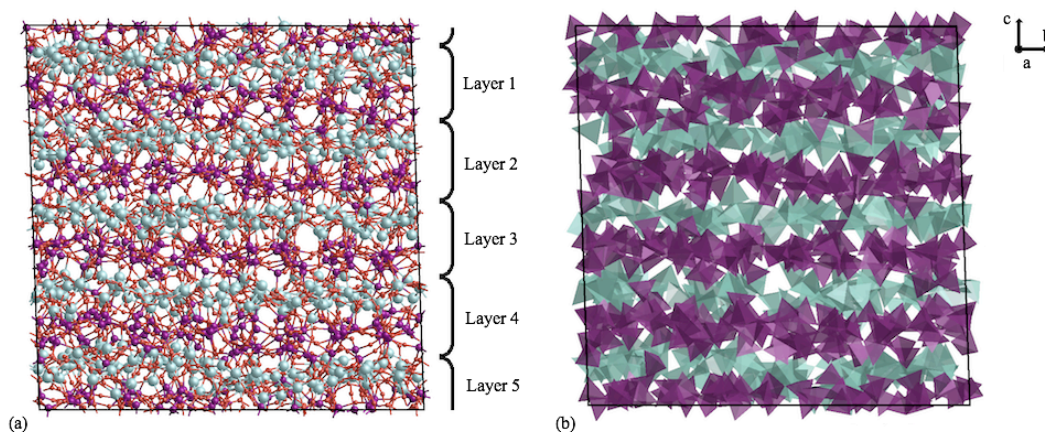


Fig. 3 (a) The fully dehydroxylated structure shows the 1:1 layering is still present. (b) Same structure with only the Si and Al polyhedra shown.

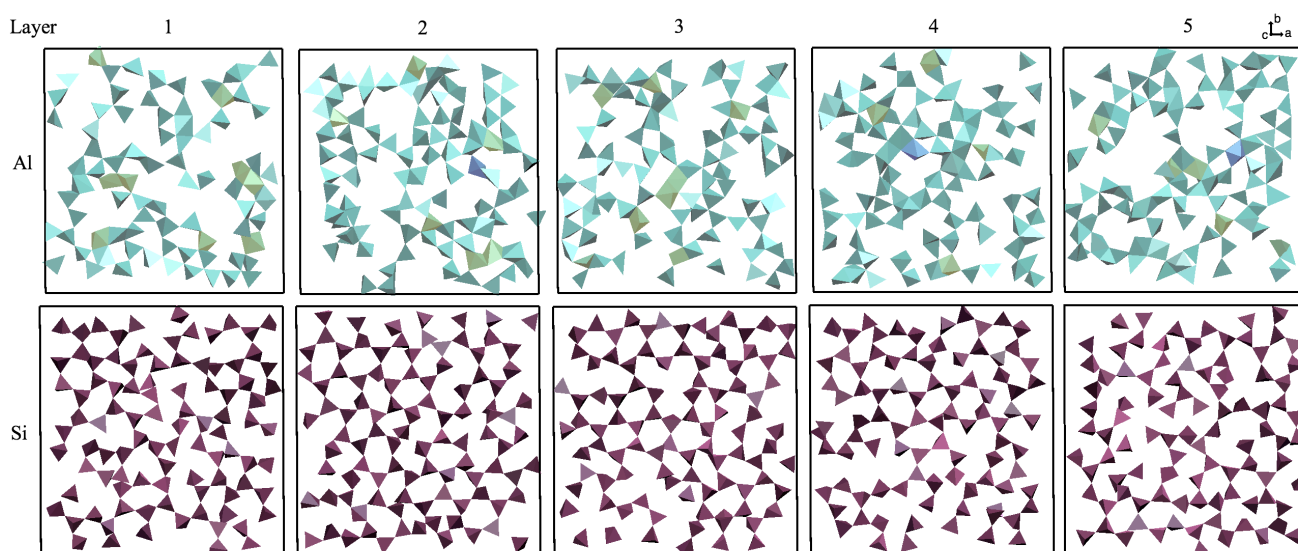


Fig. 4 Cross-sectional slices of the individual layers as you progress down the c -axis (see Fig. 3). The majority of the aluminium exists in clusters of 4-fold configurations, however, there are incidences of both 5-fold and 6-fold Al present. By comparison, the silicon layers are relatively unchanged and evenly dispersed.

In the final structure, a significant amount of distortion or ‘buckling’ is present in the layers, particularly in the aluminium layer, which was reported in the small-scale simulations^{33,34}.

In the initial stages of the dehydroxylation, the vacancies produced by the loss of hydroxyls from the structure create large distortions in the layers. These distortions are the result of what can be visualized as localized migration of the silicon and aluminium atoms out of their lattice positions and into the inter-layer space, creating bridges between the layers. These bridges are caused by different local effects. An aluminium bridge produces the most prominent effect, and is dependent on neighbouring pairs of inter-layer hydroxyls being removed i.e. two sets of adjacent hydroxyl groups reacting to form two waters and two residual oxygen atoms. The initial instability is overcome by the partial migration of the aluminium cation to an adjacent vacant site in the inter-layer space. This migration of the aluminium has been reported previously in density functional studies of the dehydroxylation of 2:1 dioctahedral aluminous clay minerals⁵. The migration in turn creates a distortion within the layer as it leaves. This combination causes the localised buckling of the layer. If another vacancy is produced in the local vicinity of this Al, it will continue to migrate along the layer. The silicon bridging is facilitated by smaller distortions in the local environment and is much less pronounced, with no migration further than the initial move into the interlayer space occurring.

Through the formation of bridges, the aluminium atoms will no longer exist in octahedral configurations. The decrease in the number of oxygen’s in the system means that returning to a six-fold coordination will not be possible, and a local system of 4- and 5- fold aluminium results. The removal of inner-layer hydroxyls further adds to the disorder within the layers, ultimately resulting in widening the layers and thus diminishing the interlayer spacing. It must also be noted that no diffusion of any cations across the layers was observed.

The final structure is shown in Fig. 3 and 4. The Al layers show a significant amount of disorder, with the majority of

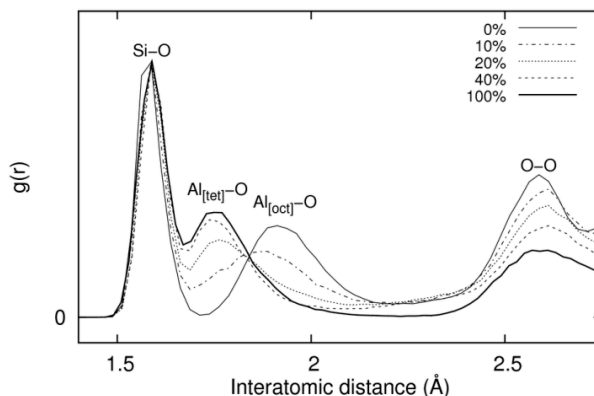


Fig. 5 Normalised calculated total radial distribution function showing the three main interactions for the dehydroxylation process. Calculated from the equilibrated structures at the end of each dehydroxylation step.

the aluminium in 4-fold coordination. The silicon layers, however, appear relatively similar with little disorder. This confirms that the structural transformation of kaolinite to metakaolin is driven by the migration and re-organisation of the aluminium layers.

The calculated radial distribution functions (RDFs) for the simulated structures are shown in Fig. 5, and provide a quantitative analysis of the structural changes. The silicon and oxygen peaks remain in the same positions, with the decrease in the oxygen-oxygen peak intensity due to the decreasing oxygen concentration in the cell. The feature of interest is the shift of the Al-O peak from 1.93 Å to 1.75 Å, which corresponds to the change in coordination from octahedral to tetrahedral. This is expected, however, there is a slight shoulder on the right of the peak that develops through the latter stages of the dehydroxylation. This may be due to the development of the 5-fold Al, which has been shown to demonstrate a peak at around 1.8 Å⁵⁰, and so further analysis of the coordination of the aluminium was conducted. The coordination of each Al atom was determined by summing the number of oxygen atoms falling within a chosen cut-off distance of 2.3 Å of that atom. This was chosen from the average minimum following the first peak in the calculated RDFs for the Al-O interactions. The change in the Al-coordination through the dehydroxylation is shown in Fig. 6. The analysis shows that there is a considerable contribution of 5-fold Al present throughout the dehydroxylation process. This corresponds with NMR studies^{26,51-53} which show an appreciable amount of 5-fold Al in samples of kaolinite calcined at temperatures ranging from 600 °C to 1000 °C.

An interesting feature from the coordination analysis is that rather than a linear relationship, the majority of the structural decomposition occurs in the removal of the first 4 steps of the dehydroxylation. Indeed, the very first step sees almost half of the octahedral aluminium transformed to 4- and 5-fold configurations equally, followed by the second step which sees more of the 6-fold Al converted to 4-fold. This trend continues until the 6th removal step where the 6-fold environment is nearly completely lost (~1%) to the 4-fold coordination (~88%), with the 5-fold coordination decreasing slightly to contributing up to 11% of the Al population. This

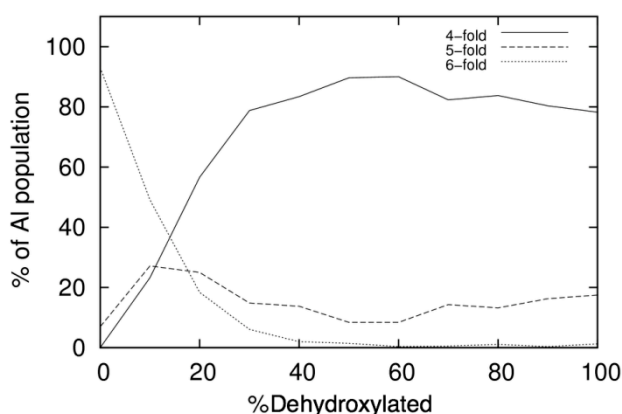


Fig. 6 Changes in aluminium coordination through the dehydroxylation process: from 6-fold to a combination of 4- and 5- fold.

corresponds to the development of a structure which has been distorted to such a degree that migration of the Al becomes impeded by the lack of suitable vacant sites. At this stage the hydroxyls in the structure can all be considered as inner-layer OH groups. In the 7th and 8th removal steps, the further dehydroxylation causes a loss of some 4-fold coordinated Al to the 5-fold

configuration. This is unexpected, as it would be expected for the loss of further oxygen's from the system to encourage the formation of the 4-fold coordinated Al over the 5-fold. However, at this stage an important aspect of the structural change must be considered. Since the hydroxyl removals are not uniform, neither will be the Al migration. In the latter stages the majority of the Al migration has already occurred, and as such the resulting aluminium layers will consist of 'clusters' of 4- and 5- fold aluminium, as can be seen in Fig 4. This clustering effect has not been previously reported, and would explain the experimentally observed lack of crystallinity in the *c*-direction of the metakaolin structure. Beyond 80% dehydroxylation, there is little change as there is not enough space left for re-organisation within the structure, and the final system consists of 74% of the aluminium population in 4-fold coordination, with 21% in 5-fold and 3% in 6-fold coordination (the remaining < 2% consists of residual Al in 3-fold coordination). White et al similarly reported a 20 % contribution of 5-fold aluminium³⁴, as well as some of the aluminium population in a planar-trigonal or 3- fold coordinated state. The presence of 3-fold aluminium reported is likely an artefact due to the small simulation cell and inter-layer spacing restraints, which do not allow the aluminium enough freedom to coordinate itself in the higher configurations that are inherently more stable.

The stability of the structure through the final stages of dehydroxylation (80% - 100%) confirms that the metakaolin structure is established prior to complete hydroxyl removal. This corresponds with experimental findings^{24,34,53} that propose that the metakaolin structure is established at this stage, with little structural change occurring beyond a structural water content of 12%.

The results show kaolinite decomposes to a structure that in all aspects discussed so far represents metakaolin, but further analysis is required before any conclusions on the structure of metakaolin can be made. In 1959 Brindley and Nakahira²¹

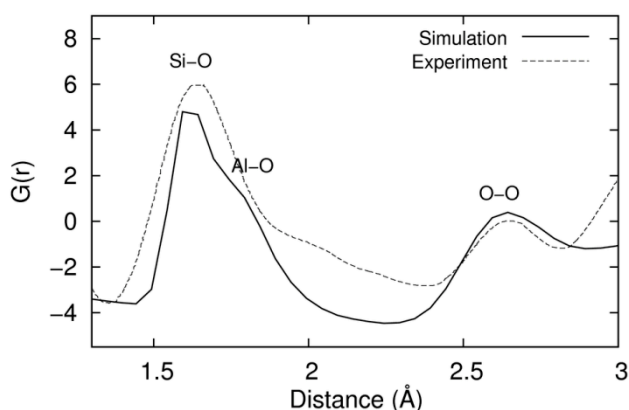


Fig. 7 Comparison of the reduced radial distribution function for the fully dehydroxylated structure compared to experimentally observed values³⁴ where $G(r) = 4\pi r \rho_o [g(r) - 1]$

proposed a set of criteria that any proposed metakaolin structure should adhere to. Several of those are relevant here, with this study confirming some of their observations. It was proposed that metakaolin should demonstrate lattice parameters that are relatively unchanged from kaolinite, but that *c*-axis periodicity should disappear. This is indeed the case in the fully dehydroxylated structure, with the cell lengths only decreasing by 5.76% from the initial kaolinite structure. The octahedral Al-O(OH) layer should also exhibit the majority of the structural re-organisation compared to the silicon layer, which has been shown in this study to be the major driving force in the structural transformation to metakaolin. Finally, the collapse of the kaolinite layers is also addressed, with the measured inter-layer spaces decreasing to between 4.86 a.u. and 6.54 a.u. depending of the degree of local buckling in the layers. This differs from the proposed value of 6.3 a.u., however, the proposed criteria do not account for the buckling effect, and as such the overall decrease observed for the density of metakaolin is maintained.

A comparison of the simulated reduced radial distribution function for the fully dehydroxylated structure compared with one obtained from experimental x-ray diffraction data³⁴ is shown in Fig. 7. The simulated metakaolin produced a Si-O interaction peak at 1.68 Å (compared to the experimental value of 1.7 Å), an Al-O peak at 1.75 Å and an O-O peak at 2.58 Å (compared with 2.6 Å). There is a shoulder on the experimental Si-O peak at approximately 2 Å that is not demonstrated in the simulated data. This could be due to octahedral Al-O in the sample, which could indicate either that the sample is not fully dehydroxylated or that there are impurities which are producing this interaction. The 4-fold Al-O interaction is clearly visible in the simulated data, but is obscured in the experimental data by the Si-O peak.

Fig. 8 shows simulated x-ray diffraction plots from the fully dehydroxylated structure at several stages through the dehydroxylation process. The sharp kaolinite peaks in the initial stages rapidly degrade into a low intensity broadened spectrum between 20 and 40 °2θ, with the kaolinite structure completely lost at 80% dehydroxylation. The broadening is demonstrated in experimental studies on metakaolin,^{18,20,23,27,29,30,33,34,47,55,56} and confirms the loss of long-range order within the structure.

Experimental diffraction patterns of metakaolin often exhibit various peaks which are attributed to impurities in the samples studies; however, the typical feature present is a broadening of the pattern, which is mirrored in the simulated pattern. Thus the structure produced from this simulation can be considered as a good representation of metakaolin.

Conclusions

This study provides a theoretical basis to understanding the atomic mechanisms underpinning the loss of crystallinity during the dehydroxylation of kaolinite to metakaolin. Through a gradual step-like removal of the hydroxyls of a simulated kaolinite model, the dehydroxylation to metakaolin has been simulated with the final structure agreeing well with experimental observations. Several groups have proposed a series of possible repeating units for metakaolin^{21,33-34}. The major flaw with these systems is that if metakaolin were constructed of a regularly repeating structure, it would be

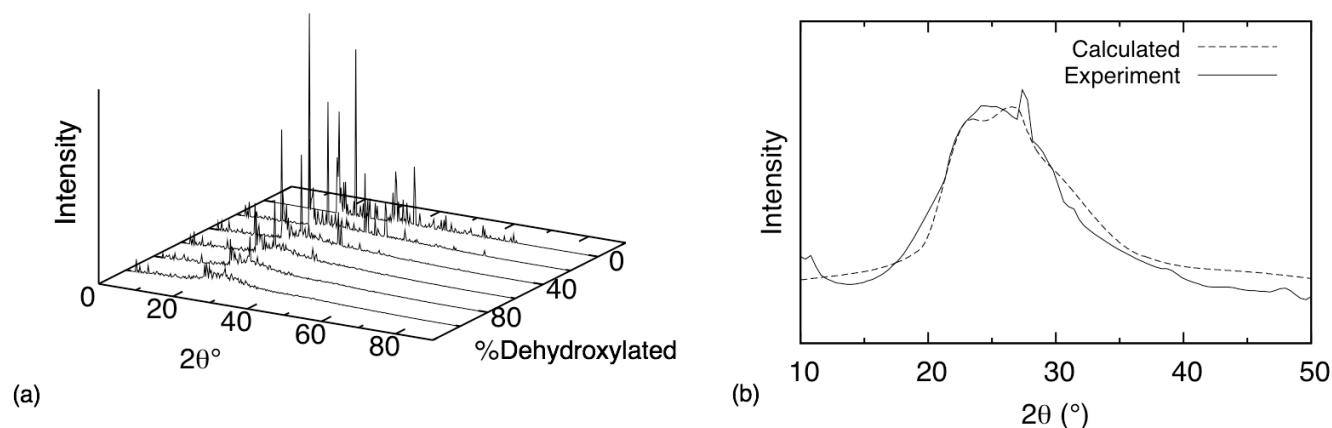


Fig. 8 (a) X-ray diffraction data calculated using the GTK Display Interface for Structures (GDIS)⁵⁴ at various stages during the dehydroxylation process using simulated $\text{CuK}\alpha$ x-ray radiation. (b) The data for the final simulated structure (simulated with a Gaussian broadening function at each point with a width of $3^\circ 2\theta$) is displayed and compared to a typical metakaolin pattern⁵⁵.

considered a crystalline material, and would behave accordingly in laboratory structural analysis measurements. This study proposes another approach to describing the structure of metakaolin. The loss of crystallinity is governed by the loss of hydroxyl groups at the surface of the inter-layer spacing, which in turn causes the migration of the aluminium into the vacant sites provided by the inter-layer space. This migration causes the buckling of the layers. The degree of buckling is significant and high resolution surface imaging of metakaolin crystals⁵⁷ show an increase in surface roughness which may be a product of this buckling effect.

The proposed structure for metakaolin shows the typical amorphous x-ray diffraction pattern; however, since no diffusion of the cations occurs across the layers, no loss in the 1:1 layering of Al-Si is present. The proposed structure of metakaolin also confirms the presence of as much as 20% of the aluminium population in 5-fold coordination. The presence of 5-fold aluminium has been demonstrated not to be a preferential configuration over others, but simply a product of the Al cations inability to migrate to more stable configurations once the layers become severely distorted.

Our results demonstrate that more than one configuration can be present within a relatively small system - the simulation cell was approx. $(36 \text{ \AA})^3$. Whilst the locations of the hydroxyl groups removed do not affect the total structural properties, the local environment can vary from aluminium rich to aluminium deficient. This will produce very different environments when metakaolin is used in chemical reactions and the varying aluminium concentrations may create areas of higher or lower reactivity. In some cases the Al may even migrate in such a way that it creates small areas demonstrating higher crystallinity, which would offer an alternative explanation to the consistent observations of crystalline peaks in the measured diffraction patterns of 'pure' metakaolin, which typically are explained away as crystalline impurities.

Acknowledgements

The authors would like to acknowledge Curtin University and the Centre for Sustainable Resource Processing for financial support. The Australian National Computing Facility and iVec are acknowledged for the provision of computational resources, and Julian Gale for the provision of and support for the GULP software. P.R. thanks the Australian Research Council for his Fellowship and support through a Discovery grant (DP0986999).

Notes and References

† Electronic Supplementary Information (ESI) available: See DOI: 10.1039/b000000x/

- 1 P. Bala, B. K. Samantaray and S. K. Srivastava, *Bull. Mater. Sci.*, 2000, **23**, 61-67
- 2 M. C. Mayoral, M. T. Izquierdo, J. M. Andres and B. Rubio, *Thermo. Acta.*, 2001, **373**, 173-180.
- 3 A. Plancon, *Amer. Miner.*, 2002, **87**, 1672-1677.
- 4 L. Wang, M. Zhang, S. A. T. Redfern and Z. Zhang, *Clays Clay Miner.*, 2002, **50**, 272-283.

- 5 S. Stackhouse, P. V. Coveney and D. M. Benoit, *J. Phys. Chem.*, 2004, **108**, 9685-9694.
- 6 B. Dubacq, O. Vidal and V. de Andrade, *Contrib. Mineral. Petrol.*, 2010, **159**, 159-174.
- 7 R. T. Cygan, J. A. Greathouse, H. Heinz and A. G. Kalinichev, *J. Mat. Chem.*, 2009, **19**, 2441-2636.
- 8 O. Vidal and B. Dubacq, *Geochim. Cosmochim. Acta*, 2009, **73**, 6544-6564.
- 9 J. Ortega-Castro, N. Hernandez-Haro, M. T. Dove, A. Hernandez-Laguna and C. I. Sainz-Diaz, *Amer. Miner.*, 2010, **95**, 209-220.
- 10 D. M. Moore and J. Hower, *Clays Clay Miner.*, 1986, **34**, 379-384.
- 11 T. C. Wu, W. A. Basset, W. L. Huang, S. Guggenheim and A. F. Koster van Groos, *Amer. Miner.*, 1997, **82**, 69-78.
- 12 S. Guggenheim and K. A. van Groos, *Clays Clay Miner.*, 2001, **49**, 433-443.
- 13 L. J. Michot, I. Bihannic, M. Pelletier, E. Rinnert and J. L. Robert, *Amer. Miner.*, 2005, **90**, 166-172.
- 14 E. Ferrage, C. Tournassat, E. Rinnert, L. Charlet and B. Lanson, *Clay Miner.*, 2005, **53**, 348-360.
- 15 E. Ferrage, B. Lanson, B. A. Sakharov, N. Geoffroy, E. Jacquot and V. A. Drits, *Amer. Miner.*, 2007, **92**, 1731-1743.
- 16 O. Castelein, B. Soulestin, J. P. Bonner and P. Blanchart, *Ceram. Inter.*, 2000, **27**, 517-522.
- 17 C. Y. Chen, G. S. Lan and W. H. Tuan, *Ceram. Inter.*, 2000, **26**, 715-720.
- 18 Y. F. Chen, M. C. Wang and M. H., Hon, *J. Eur. Ceram. Soc.*, 2004, **24**, 2389-2397.
- 19 K. Okada, N. Otsuka and J. Ossaka, *J. Amer. Ceram. Soc.*, 2005, **69**, 251-253.
- 20 N. Tezuka, I. M. Low, I. J. Davies, M. Prior and A. Studer, *Physica B*, 2006, **385-386**, 555-557.
- 21 G. W. Brindley and M. Nakahira, *J. Amer. Ceram. Soc.*, 1959, **42**, 314-318.
- 22 G. B. Mitra and S. Bhattacharjee, *Amer. Miner.*, 1969, **54**, 1409-1418.
- 23 G. B. Mitra and S. Bhattacharjee, *Acta Cryst.*, 1970, **B26**, 2124-2128.
- 24 T. W. Davies and R. M. Hooper, *J. Mat. Sci. Lett.*, 1985, **4**, 39-42.
- 25 K. J. D. MacKenzie, I. W. M. Brown, R. H. Reinhold, and M. E. Bowden, *J. Amer. Ceram. Soc.*, 1985, **6**, 293-297.
- 26 J. Rocha and J. Klinowski, *Phys. Chem. Miner.*, 1990, **17**, 179-186.
- 27 J. Rocha, J. M. Adams and J. Klinowski, *J. Solid State Chem.*, 1990, **89**, 260-274.
- 28 A. Ortega, F. Rouquerol, S. Akhouayri, Y. Laureiro and J. Rouquerol, *Appl. Clay Sci.*, 1993, **8**, 207-214.
- 29 M. Belloto, A. Gualtieri, G. Artioli and S. M. Clark, *Phys Chem Miner.*, 1995, **22**, 207-214.
- 30 R. L. Frost and A. M. Vassallo, *Clays Clay Miner.*, 1996, **44**, 635-651.
- 31 A. Gualtieri and M. Belotto, *Phys. Chem. Miner.*, 1998, **25**, 442-452.
- 32 P. Ptacek, D. Kubatova, J. Havlica and J. Brandstetr, *Thermo. Acta*, 2010, **501**, 24-29.
- 33 C. E. White, J. L. Provis, T. Proffen, D. P. Riley and J. S. J. van Deventer, *Phys. Chem. Chem. Phys.*, 2010, **12**, 3239-3245.
- 34 C. E. White, J. L. Provis, T. Proffen, D. P. Riley and J. S. J. van Deventer, *J. Phys. Chem. A.*, 2010, **114**, 4988-4996.
- 35 D. M. Teter (private communication).
- 36 A. N. Cormack, J. Du and T. R. Zeitler, *Phys. Chem. Chem. Phys.*, 2002, **4**, 3193-3197.
- 37 A. Tilocca and N. H. de Leeuw, *J. Mat. Chem.*, 2006, **16**, 1950-1955.
- 38 A. Tilocca, N. H. de Leeuw and A. N. Cormack, *Phys. Rev.*, 2006, **73**, 104209.
- 39 J. Du, R. Devanathan, L. R. Corrales, W. J. Weber and A. N. Cormack, *Phys. Rev. B*, 2006, **74**, 214204.
- 40 B. J. Teppen, K. Rasmussen, P. M. Bertsch, D. M. Miller and L. Schafer, *J. Phys. Chem. B*, 1997, **101**, 1579.
- 41 R. T. Cygan, J. L. Liang and A. G. Kalinichev, *J. Phys. Chem. B*, 2004, **108**, 1255.
- 42 J. A. Greathouse, J. S. Durkin, J. P. Larentzos and R. T. Cygan, *J. Chem. Phys.*, 2009, **130**, 134713.
- 43 D. L. Bish, *Clays Clay Miner.*, 1993, **41**, 738.
- 44 J.D. Gale and A.L. Rohl, *Mol. Simul.*, 2003, **29**, 291-341.
- 45 T. J. Ahrens, *Mineral Physics and Crystallography: A Handbook of Physical Constants*, American Geophysical Union: Washington, DC, 1995.
- 46 W. Smith, *Mol. Simul.*, 2006, **32**, 933-1121.
- 47 Z. Zhang, X. Yao, H. Zhu, S. Hua and Y. Chen, *Journal of Wuhan University of Technology – Mater. Sci. Ed.*, 2009, **24**, 132-136.
- 48 C. E. White, J. L. Provis, D. P. Riley, G. J. Kearley and J. S. J. van Deventer, *J. Phys. Chem.*, 2009, **113**, 6756-6765.
- 49 N. H. Mondol, J. Jahren and K. Bjorlykke, *The Leading Edge*, 2008, **27**, 758-770.
- 50 B. T. Poe, P. F. McMillan, C. A. Angell and R. K. Sato, *Chem. Geol.*, 1992, **96**, 333-349.
- 51 J. Sanz, A. Madani, J. M. Serratos, J. S. Moya and S. Aza, *J. Amer. Ceram. Soc.*, 1988, **71**, 418-421.
- 52 J. F. Lambert, W. S. Millman and J. J. Fripiat, *J. Amer. Chem. Soc.*, 1989, **111**, 3517-3522.
- 53 R. H. Meinhold, R. C. T. Slade and T. W. Davies, *Appl. Magn. Reson.*, 1993, **4**, 141-155.
- 54 S. Fleming and A. Rohl, *Z. Krist.*, 2005, **220**, 580-584.
- 55 M. H. Zhang and V. M. Malhotra, *Cem. Concr. Res.*, 1995, **25**, 1713-1725.
- 56 L. Heller-Kallai and I. Lapidés, *Appl. Clay Sci.*, 2007, **35**, 99-107.
- 57 A. Mikowski, P. Soares, F. Wypych, J.E.F.C. Gardolinski and C. M. Lepienski, *Philosophical Magazine*, 2007, **87**, 4445-4459.